

A revision on Rayleigh capillary jet breakup

Alfonso M. Gañán-Calvo^{1, 2}

¹⁾*Dept. Ing. Aeroespacial y Mecánica de Fluidos, Universidad de Sevilla.*

Camino de los Descubrimientos s/n 41092, Spain.

²⁾*Laboratory of Engineering for Energy and Environmental Sustainability, Universidad de Sevilla, 41092, Spain.*

(*Electronic mail: amgc@us.es)

(Dated: 25 October 2022)

The average Rayleigh capillary breakup length of a cylindrical Newtonian viscous liquid jet moving with homogeneous velocity \hat{U} (negligible external forces) must be determined by the selection of normal modes with time-independent amplitude and wavelength (invariant modes, IMs). Both positive and negative group velocity IMs exist in ample ranges of the parameter domain (Weber and Ohnesorge numbers), which explains (i) the average breakup length independence on ambient conditions (long-term resonance), and (ii) its proportionality to the inverse of the spatial growth rate of the dominant positive group velocity IM. Published experimental results since Grace (1965, PhD Thesis) confirm our proposal.

PACS numbers: 47.55.D-, 47.55.db, 47.55.df

Capillary viscous liquid jets are ubiquitous fluid structures in nature and technology, with an immense literature devoted to them (we save space and time to the reader by referring to a couple of reviews^{1,2}). Their intrinsically unstable nature, leading to their eventual breakup into droplets, can be rigorously studied via analytical linear instability analysis whenever their basic unperturbed state with negligible external forces (for example, when gravity is negligible compared to capillary forces) can be consistently reduced to an infinite capillary cylindrical Newtonian liquid column of radius R . The normal mode analysis with varicose ($m = 0$) perturbations of the form $e^{i(kz - \Omega t)}$ leads to a dispersion relationship that can be canonically expressed as^{3,4}:

$$\Delta(\Omega, k) = (k^2 + \chi^2)^2 \frac{I_0(k)}{I_1(k)} - 4k^3 \chi \frac{I_0(\chi)}{I_1(\chi)} + k(2(k^2 - \chi^2) + (k^2 - 1)/Oh^2) = 0, \quad (1)$$

with $\chi = (k^2 - i\Omega/Oh)^{1/2}$, where $Oh = \mu/(\rho\sigma R)$ is the Ohnesorge number, and ρ , μ and σ are the liquid density, viscosity and surface tension, respectively. Lengths and times are made dimensionless with R and $(\rho R^3/\sigma)^{1/2}$, respectively.

Assuming that the liquid column is moving at a homogeneous speed \hat{U} , Doppler and spatial growth effects that are absent in (1) must be considered. These effects are incorporated exactly making $\Omega = \omega - kU$ (Keller's transformation⁵) and considering $\omega = \omega_r + i\omega_i$ and $k = k_r + ik_i$ complex in (1) (spatiotemporal instability analysis), where $U = We^{1/2}$ and $We = \rho\hat{U}^2 R/\sigma$. Thus, the dispersion relationship (1) defines a five-dimensional manifold in the general six-dimensional real space $\{Oh, U, \omega_r, \omega_i, k_r, k_i\}$ which comprises the whole normal mode spectrum.

The linear wave nature of spatiotemporal normal modes imply the concept of group velocity⁶, defined from (1) as⁷:

$$W = d\omega/dk = -(\partial_k \Delta)/(\partial_\omega \Delta). \quad (2)$$

In conservative dispersive media, it coincides with the velocity of energy transport, but not in dissipative media (e.g. with viscous damping) where W is generally complex. Its real and imaginary parts $W = U_g + iU_d$ (i.e. $U_g = \text{Re}(d\omega/dk)$ and $U_d = \text{Im}(d\omega/dk)$) have kinematic interpretations^{8,9} as the envelope propagation velocity of a wave packet with central wavenumber k and the temporal drift experienced by that wavenumber, respectively. Interestingly, it has been shown⁹ that in those dissipative media where W can be real (i.e. those that can exhibit waves whose wavenumber has no temporal drift), $W = U_g$ and coincides with the propagation velocity of energy as in nondissipative

media. An infinite cylindrical capillary viscous liquid column moving with uniform speed U is an example of such media, and this work aims to exploit its physical implications.

The group velocity concept^{10–12} and Keller's transformation allowed Leib and Golstein¹³ to describe the spatiotemporal convective-absolute (C-A) instability limit in terms of a marginal mode $\{\omega^*, k^*\}$ such that its temporal growth rate and group velocity are zero¹¹: $\omega_i|_{k^*} = 0$, $U_g = \text{Re}(d\omega/dk)|_{k^*} = 0$ and $U_d = \text{Im}(d\omega/dk)|_{k^*} = 0$, respectively. These conditions together with Cauchy-Riemann ones imply that $\partial\omega_r/\partial k_r|_{k^*} = \partial\omega_r/\partial k_i|_{k^*} = 0$ with $\omega_i = 0$, from which the classical saddle-point criteria immediately follows. This defines the marginal Leib-Goldstein (L-G) curve $U = U^*(Oh)$ in the $\{Oh, U\}$ domain.

Once in the convective instability domain ($We > We^*$ or $U > U^*$), the observed long-term natural breakup regime of a steady cylindrical viscous capillary jet, with a relatively narrow range of breakup lengths, suggests a causal argument: the *average* long-term breakup length must be determined by the normal modes with time-independent local amplitude and wavelength (i.e. *invariant modes*, IMs), and positive downstream spatial growth rate. Thus, the IMs must satisfy three fundamental conditions for long-term dominance:

- (i) $\omega_i = 0$ (time-independent local amplitude),
- (ii) $\text{Im}(d\omega/dk) = 0$ (no spatial drift of its wavelength^{8,9}), and
- (iii) $k_i < 0$ (i.e. $-k_i$ positive according to the sign criteria here adopted).

In physical terms, the long-term condition (ii) automatically imply that the group velocity of IMs is their velocity of energy transport. In mathematical terms, the IMs comprise a range (or sub-manifold) of the full modal spectrum of the system. Such a sub-manifold materializes as a four-dimensional sheet in the five-dimensional space of normal modes. However, there are no restrictions on the sign of the group velocity in this sub-manifold. Figure 1 represents the locations of the IM sub-manifold in the parameter space. Figures 1(a) and (b) gives projections on the $\{Oh, U\}$ plane of the sheet of forward ($U_g > 0$) and backward ($U_g < 0$) IMs, respectively: the plots provide the values of the group velocity U_g of IMs as a function of Oh and U . Noteworthy, at least one *negative* group velocity (or backward) IM can be found for given $\{Oh, U\}$ values in addition to the always present positive group velocity (or forward) IM (see figure 1 for $U > U^*$). Thus, the energy can be effectively transported backward and forward along the capillary jet by the IMs, independently of their phase speed ω_r/k_r and spatial growth rate.

A fundamental causal condition in long-term breakup from a fixed source (nozzle) is that the normal mode that is eventually selected, responsible for the average breakup length and size of resulting droplets, must have a *positive real group velocity*. We call it the *dominant* IM (or DIM).

Thus, the spectrum of backward IMs can propagate energy upstream from the breakup region while the forward DIM that determines the most likely breakup length sweeps that energy toward the rupture. Thus, in the absence of any external energy input (except the steady injection of kinetic and surface energy from the source), if the same long-term steadiness assumption applied to mode selection is considered for the flow of energy along the jet, the perturbation at the source must not be arbitrary but self-imposed by the breakup dynamics (the only source of perturbations). Consequently, in the parametrical subdomain of $\{Oh, U\}$ defined by those values contained in the four-dimensional sub-manifold of IMs represented in figure 1 where both forward and backward IMs exist, we propose that the breakup length L_j must be

- (1) the result of a long-term mechanical *resonance*, where the DIM is the main selected breakup mode, and
- (2) proportional to the spatial growth rate $-k_i^*$ of the DIM, i.e.

$$L_j = -C/k_i^*. \quad (3)$$

C must be a constant that may depend on the geometry of the jet source, where the flow of backward energy is choked and scattered¹⁴ by the boundary conditions at the nozzle. That was the main claim of a recent work¹⁵ from rather general experimental observations, in line with the suggestions implied by others¹⁶, in particular from Umemura^{17,18}. In a recent work Liu et al.¹⁹ have beautifully proved the validity of previous assumptions by introducing a continuous controlled energy excess by a laser beam aimed at a narrowly selected position of the jet close to the natural breakup point. It should be emphasized that the introduced energy was not oscillatory. The authors show that the system locks-in: the energy introduced is primarily absorbed by the invariant modes

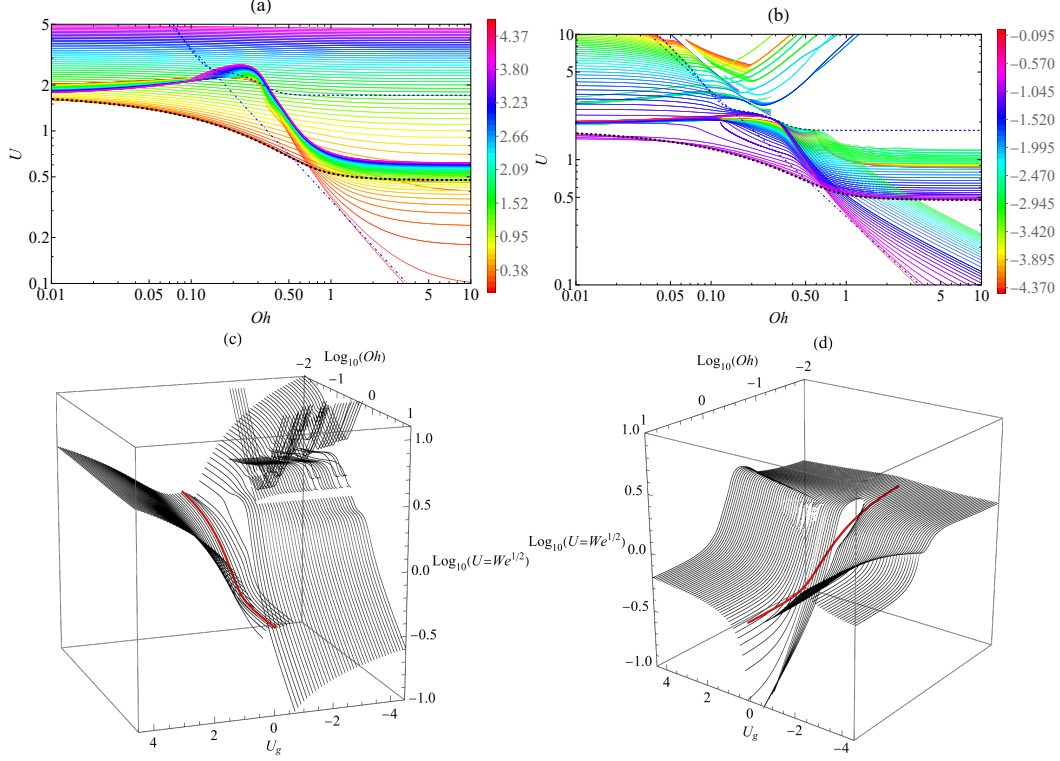


FIG. 1. (a) and (b): Values of the positive (a) and negative (b) group velocity ($U_g = \text{Re}(d\omega/dk) < 0$) IMs on the $\{Oh, U\}$ plane. The color bar gives the values of U_g . The black dashed line is the Leib-Goldstein C-A marginal stability limit ($\omega_i = 0$, $d\omega/dk = 0$). The dashed blue lines in (a) and (b) are the upper U^{**} values over which no backward IM is generally found. The dot-dashed blue line is an eye-guide for the minimum U^{***} below which no forward DIM is found for $Oh \gtrsim 0.7$. Note that the range of group velocities shown is limited to $-5 < U_g < 5$. (c) and (d) Three-dimensional views of the upper and lower sides of the sheet, with lines of constant U_g values, showing the existence of multiple modes for a range of $\{Oh, U\}$ values. Observe the branch-cut topology that connects both sides of the sheet at the central eyelet. The red line is the C-A marginal stability limit.

that become amplified over the whole the spectrum, and consequently the breakup turns regular. The “enhanced breakup” length decreases compared to the natural one¹⁹ due to the energy excess put in the DIM.

Subsequent discussion and consistency of the proposal. - With the exception of a highly damped forward IM in a narrow region of the $\{Oh, U\}$ space (figure 1(a)), the group velocity of the DIM (upper side of the sheet) exhibits a monotonous dependency with $\{Oh, U\}$ that asymptotically approaches U . In contrast, the backward IMs show a greater complexity, with visible edges that degenerate into separate bangs perpendicular to the $\{Oh, U\}$ plane (i.e. their projections on the $\{Oh, U\}$ plane are lines). These features can be observed in the three-dimensional views of figures 1(a) and (b) given in figures 1(c) and (d). The dashed black lines in figures 1(a) and (b) (red lines in (c) and (d)) are the marginal C-A instability limit.

The fundamental result here is that at least a negative group velocity mode can be found in a continuous subdomain of $\{Oh, U\}$ values with $U^* < U < U^{**}$ above the C-A marginal stability limit, where U^{**} is the upper limit of U in the $\{Oh, U\}$ space where both forward and backward IMs exist. Figures 1(a) & (b) show that upper U^{**} limit by a blue dashed line. Interestingly, that line asymptotically approaches $U^{**} \rightarrow 0.4Oh^{-1}$, or equivalently, $Ca = U \cdot Oh \rightarrow Ca^{**} = U^{**} \cdot Oh = 0.4$.

However, for $U \gtrsim U^{**}$, no negative group velocity invariant modes can be found. In this regard, the streaks with slope 1 shown for $U > U^{**}$ are the projections of the bangs previously mentioned, which have virtually no area in the $\{Oh, U\}$ plane and therefore do not offer any effective vehicle

for backward energy transmission. In this case, although the breakup mode selection criteria are maintained, the sensitivity of the breakup length to external perturbations may significantly increase. Thus, extremely long jets can be expected under carefully maintained ballistic conditions in vacuum, in contrast to the independency of the breakup length on the surrounding gas density in the Rayleigh regime within the subdomain $U^* < U < U^{**}$. This was early observed experimentally and reported in detail by Grant²⁰, Grant & Middleman²¹ and Fenn & Middleman²². Noteworthy, in the recent work of Liu et al.¹⁹ the maximum value of Oh is below 0.05, with U below U^{**} , and therefore the presence of backward invariant modes was guaranteed in those experiments, leading to resonance.

Besides, one may find forward IMs below the marginal C-A U^* limit for $Oh \gtrsim 0.7$, see the region between U^{**} and $Ca^{***} = U^{**} \cdot Oh = 0.35$ (blue dashed and dot-dashed lines, respectively) in figure 1. First, one can verify that their group velocity is always smaller than the group velocity (in absolute value) of the corresponding backward IM (see figure 1), and more importantly, the phase velocity ω_r/k_r of at least one of those backward IMs is in effect negative, as shown in figure 2, and therefore the jet may become absolutely unstable. However, to have a negative phase speed does

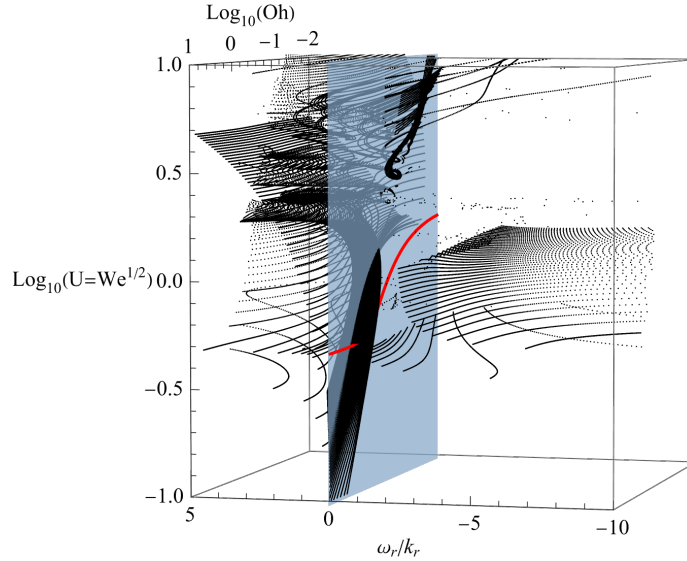


FIG. 2. Phase speed ω_r/k_r of IMs in the $\{Oh, U\}$ domain explored. The virtual lines visualized correspond to the constant U_g values of figure 1. The blue plane is $\omega_r/k_r = 0$.

not necessarily lead to absolute instability if the upstream spatial decay (or upstream spatial growth rate) $-k_i$ of the corresponding mode is larger than the one of the forward DIM. Thus, a detailed analysis of $-k_i$ becomes necessary.

The topological complexity of the IM sheet giving the growth rate values $-k_i$ is apparent in the three dimensional views of figures 3(a) and (b). In a first inspection, one observes that the values of $-k_i$ become smaller for the set of DIMs in figure 1(a) than the corresponding ones of the backward IMs in figure 1(b), for $U^{***} < U < U^*$ and $Oh > 0.7$. Thus, the DIMs sweep downstream the energy from farther upstream than the distance of penetration of the corresponding backward IMs. In addition, one could see in figure 2 that those DIMs have phase speeds significantly larger than the backward IMs. In consequence, one may expect to find convectively stable viscous jets in the range $U^{***} < U < U^*$ with $Oh > 0.7$. In reality, this does not contradicts the analysis carried out by Leib and Goldstein¹³ since their work was restricted to Oh values in the range $0.008 < Oh < 0.164$. Further careful experimental work in vacuum is needed to confirm whether the actual stability limit for $Oh > 0.7$ would be $U^{***} = 0.35/Oh$ instead of the marginal C-A limit resulting from a continuous extension of Leib and Goldstein's original Oh range.

Another fundamental feature of IMs is that their $-k_i$ reach extreme values in the $\omega_i = 0$ spectrum. This is demonstrated in the Appendix A. First, causal arguments (boundary conditions at the source) lead to consider negative k_i values (i.e. positive growth rate in the direction of $\hat{U} > 0$ only) and decaying or zero temporal growth $\omega_i \leq 0$ modes only. Simple inspection shows that k_i is minimum

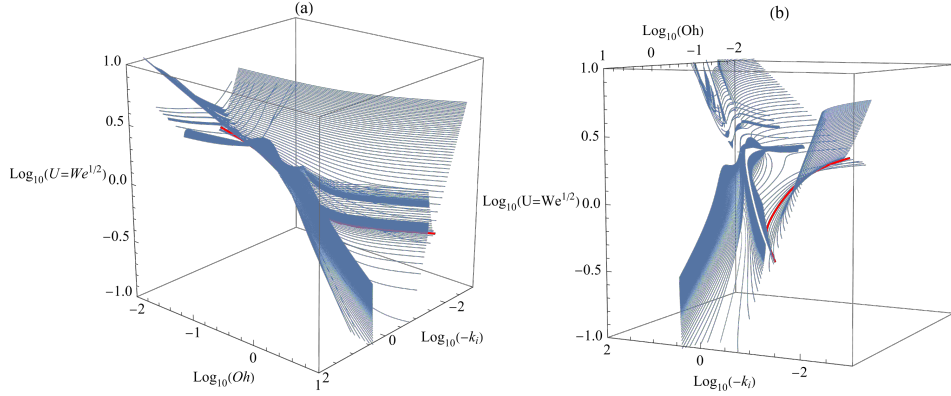


FIG. 3. (a) & (b) Complete three-dimensional views from different angles of the spatial growth rate $-k_i$ sheet, as a function of $\{Oh, U\}$. The sheet is visualized by the same U_g iso-contours of figure 1. The red line is the C-A marginal stability limit ($d\omega/dk = 0$, $\omega_i = 0$).

(maximum $-k_i$ growth rate, see figure 7, Appendix A) for the DIM ($U_d = 0$, $U_g > 0$). In contrast, the growth rate $-k_i$ is minimum for backward IMs. This means that backward IMs drive energy farther upstream (smaller $-k_i$) than the ones with non-zero $\text{Im}(d\omega/dk)$ (i.e. modes with temporal drift of their wavenumber). Even more interestingly, one can verify that the whole backward mode spectrum have temporally decaying modes ($\omega_i < 0$) with spatial growth $-k_i$ smaller than the locally long-term invariant ones ($\omega_i = 0$), independently of their propagation speed ω_r/k_r . Therefore, those latter modes penetrate farther upstream conveying the unsteady energy from the breakup region.

In addition, the only modes with larger spatial growth rate than the DIM are all temporally decaying modes ($\omega_i < 0$). Interestingly, one finds for the same initial amplitude that $e^{(-k_i + \omega_i U)z} > e^{-k_i^* z}$, i.e. $-k_i + k_i^*$ is slightly larger than $-\omega_i/U$ for these decaying modes. However, they cannot overcome the DIM in the long run since the backward energy from each breakup event that would feed those modes is injected during a short fraction of the average breakup period. In fact, the existence of these spatially faster growing but temporally decaying modes is the only reason why a rather *chaotic* short-term natural breakup is observed, rather than a perfectly regular breakup as one would expect from a short-term perfect resonance with a single overall dominant mode¹⁹. This is a beautiful illustration of the maintenance of a certain level of chaos in many natural mesoscale processes. This is also the reason why a regular breakup is possible with excitation frequencies ω_r different from the one of the DIM, ω_r^* , if the excitation energy (or initial amplitude) is large enough for that specific mode^{23–28}. The only possible short-term resonance without an oscillating excitation must be in those conditions when a continuous energy input is specifically absorbed by the DIM, like in the experiments of Liu et al.¹⁹. The consistency of these observations makes the self-sustained long-term (average) invariant breakup hypothesis for $U^* < U < U^{**}$ hardly refutable, even in the total absence of any outer noise or thermal fluctuations^{15,17}.

It is important to note that the values of the spatial wavenumber k_r^* of the DIM are close (but *not equal*¹⁴) to the ones of the more classical and simpler temporal stability analysis^(4,29), with no U involved). This justifies the success of the latter and the applicability of the Rayleigh prediction to the expected droplet size at breakup. In fact, the spatial growth rate $-k_i^*$ of the DIM can be expressed as $-k_i^* = \Omega_i^*/U$ using Keller's transformation with $\omega_i = 0$, where Ω_i^* would be the observed temporal growth rate of the DIM in a fixed frame where the jet moves with speed U . However, Ω_i^* does not coincide with the maximum temporal growth rate Ω_i^{max} of the temporal analysis, except in the $U \rightarrow \infty$ limit, as noted by Leib and Goldstein¹⁴: note that the temporal analysis implicitly assumes $k_i = 0$ (i.e. temporal analysis assumes a real k in (1), only).

Experimental validation of the proposal. - To perform an efficient comparison with experiments, note that the two-dimensional dependence of the DIM's wavenumber $k_i = k_i^*(Oh, U)$, shown in figure 4, exhibits an interesting regularity that was already suggested in the temporal analysis of Weber³. In fact, a single variable $\zeta = 2U(1 + c_\mu Oh)$ was already present in that temporal analysis: the optimum wavenumber (very close to that of the spatiotemporal DIM) and the maximum temporal

growth can be expressed under a rather general approximation as $k_r^{opt} = \zeta^{-1/2}$ and $\Omega_i^{max} = c_\omega^{-1} \zeta^{-1}$, with $c_\mu = (9/2)^{1/2}$ and $c_\omega = 2^{1/2}$. Translated to our spatiotemporal analysis with $\omega_i = 0$, and assuming $\Omega_i^{max} \simeq \Omega_i^*$, one can express $\Omega_i^* = -U k_i^* \simeq 2^{-1/2} \zeta^{-1}$ (the larger U , the more exact the latter).

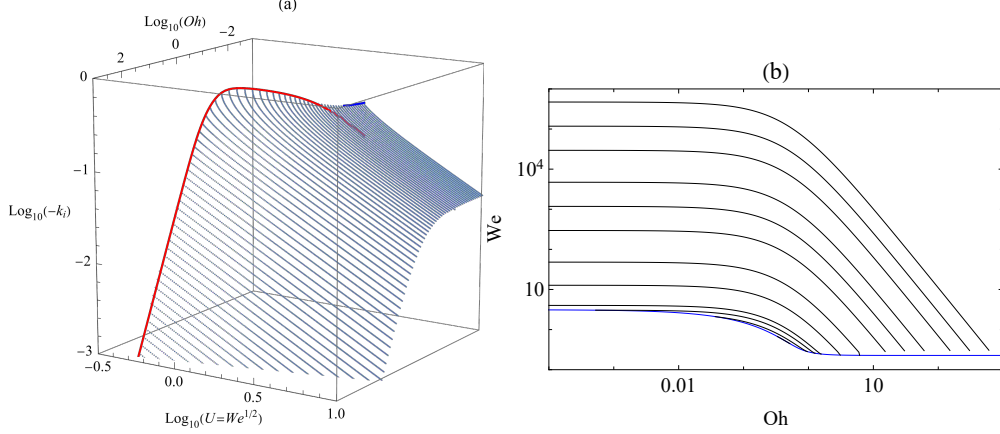


FIG. 4. Values of the spatial growth rate $-k_i^*$ for the positive group velocity $U_g > 0$ dominant mode (DIM) with $\omega_i = 0$. (a) Three dimensional view showing $-k_i^*$ values for Oh - iso-contours. The red line is the C-A marginal stability limit given by $\omega_i = 0$ and $d\omega/dk = 0$. The blue lines are the more restrictive $U_g = 0$ boundaries of the $\{Oh, U\}$ domain where the DIM exists (i.e. for $U_g \geq 0$). (b) Iso-contours of constant k_i values: $-k_i^{-1} = \{2, 3, 4, 5, 10, 20, 50, 100, 200, 500, 1000, 2000\}$. The uppermost line is for $-k_i^{-1} = 2000$; the line for $-k_i^{-1} = 2$ is nearly indistinguishable from the marginal C-A instability limit (blue line).

Actually, the reduction of the dependency $-k_i^{-1} = f(Oh, U)$ to a single-variable one as $-k_i^{-1} = f(\zeta)$ with $\zeta = 2U(1 + c_\mu Oh)$ was used in many subsequent works^(15,21,22), among many others) to approximate the breakup length $L_j = -Ck_i^{-1}$, with c_μ as a fitting constant. Although we stress again that the DIM does not coincide with the optimum temporal mode with maximum growth rate, the approximations introduced by Weber and the use of a single variable ζ are sufficiently good to collapse all points shown in figure 4(a) into an approximately single curve. The simultaneous best collapse and best fit (black dashed line) to an expression of the form $f(\zeta) = c_\omega \zeta (1 - (\zeta_0/\zeta)^\delta)^{1/\delta}$ with Weber's $c_\mu = (9/2)^{1/2}$ and $c_\omega = 2^{1/2}$ gives $\delta \simeq 2.33$ and $\zeta_0 \simeq 2.5$ using least squares and maximum regression parameter R^2 in the range $We^* < We < 40$. The resulting optimum collapse is shown in Figure 5(a). Figure 5(b) shows the relative errors committed by the obtained fitting

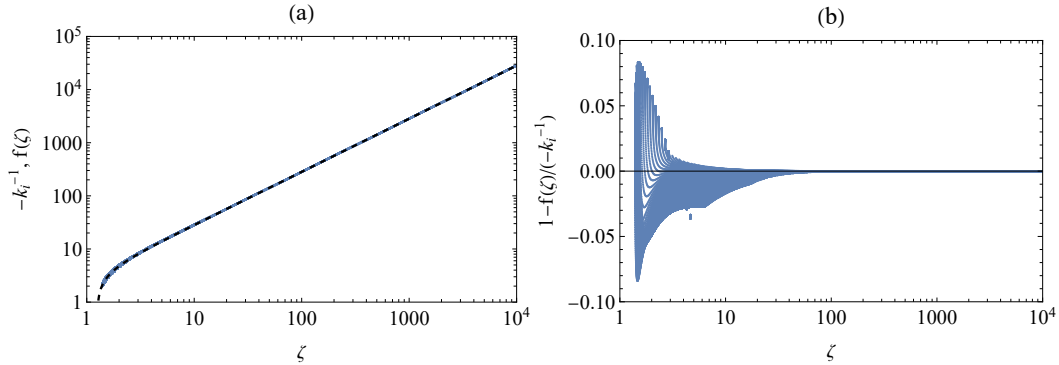


FIG. 5. (a) Values of the approximate function $f(\zeta)$, with $\zeta = 2U(1 + c_\mu Oh)$ (black dashed line), compared to the $(-k_i^*)^{-1}$ values in the range $10^{-3} < Oh < 10^3$ and $We^* < We < 40$. (b) Relative errors between $(-k_i^*)^{-1}$ values and $f(\zeta)$.

function $f(\zeta)$.

In figure 6, we compare our predictions with (i) the classical experiments from²⁰, (ii) the recently published detailed experiments in microgravity of Umemura¹⁷, and (iii) those in¹⁵ for jets from a tube. Two data from Liu et al.¹⁹ for natural and self-excited jets from a tube are also shown. The physical properties of the liquids used, nozzle diameters and geometries, etc. can be seen in the respective works and are not given here for economy. The theoretical curves with constants $C = 7.5$, 10.5 and 15.5 are plotted for comparison. The classical results of Grant²⁰ (summarized in²¹) are of particular interest here: first, he reported the insensitivity of the Rayleigh breakup length to the external atmosphere in a parametric range that can be checked to be within $U^* < U < U^{**}$, and second, a dramatic increase in sensitivity with the external atmosphere was observed for $Oh \gtrsim O(1)$ and $U > U^{**}$, confirming our proposal.

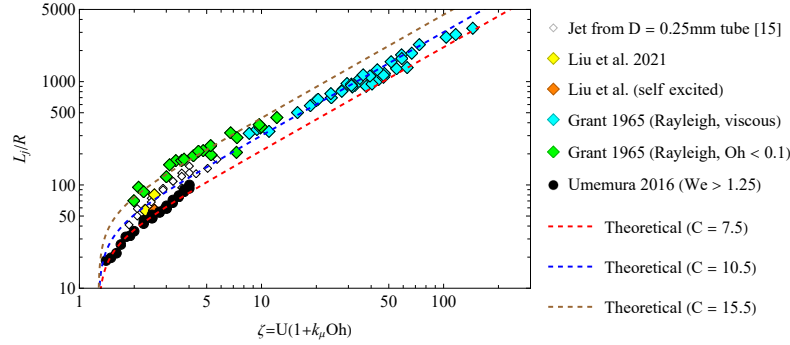


FIG. 6. Experimental data from compared to function $f(\zeta) \times C$, for two values of C .

While an excellent agreement is seen with the data of Umemura¹⁷ for $C = 7.5$, where the plug velocity is reached much earlier than in the tube experiments, the data from Grant²⁰ (jets from capillary tubes) exhibit interesting features: (i) the constant C is larger for tubes than for the orifice experiments, and (ii) C is larger for smaller viscosities. The explanation lies in the jet profile along the axial coordinate, which is clearly convergent in the experiments of Grant during a significant fraction of the total jet length until it reaches a nearly homogeneous (ballistic) diameter and velocity profiles. That homogeneity is reached earlier when the viscosity is larger, which explains the smaller C in those cases. The largest values of C correspond to low viscosity jets for which the initial relaxation length can be above 40% of the total intact length. If this initial length could be systematically excluded, the predicted length of the cylindrical jet here proposed would approach the experimental measurements of Umemura¹⁷. However, this analysis implies a systematic determination of the zero-th order steady solution as function of Oh and U beyond the scope of present work.

ACKNOWLEDGMENTS

This work was supported by the Ministerio de Economía y Competitividad (Spain) (project PID2019-108278RB) and the Junta de Andalucía (project P18-FR-3375). Lengthy and enriching discussions with profs. M. A. Herrada, J. M. López-Herrera and J. Eggers are gratefully acknowledged.

DATA AVAILABILITY STATEMENT

The data that support the findings of this study are available from the corresponding author upon reasonable request.

Appendix A

Current understanding is that the long-term breakup mode selection is determined by the *spatial* instability analysis, which restricts the mode spectrum to those modes with $\omega_i = 0$ (e.g.³⁰). The dominant mode selection immediately follows from the physical consideration of the maximum (downstream) spatial growth rate $-k_i^{max, spatial}$. The rigorous form of the *spatiotemporal* mode selection criterion here proposed, i.e. the positive group velocity mode with $\omega_i = 0$ and $U_d = \text{Im}(d\omega/dk) = 0$, leads to the same result exactly, i.e. $k_i^{max, spatial} = k_i^*$. In effect, equation (1) implies that

$$\begin{aligned} d\omega/dk &= -(\partial_k \Delta)/(\partial_\omega \Delta) = \\ &= \frac{-(\partial_{k_r} \Delta_r \partial_{\omega_r} \Delta_r + \partial_{k_r} \Delta_i \partial_{\omega_r} \Delta_i)}{|\partial_{\omega_r} \Delta|^2} \\ &+ i \frac{(\partial_{k_r} \Delta_r \partial_{\omega_r} \Delta_i + \partial_{k_r} \Delta_i \partial_{\omega_r} \Delta_r)}{|\partial_{\omega_r} \Delta|^2}, \end{aligned} \quad (\text{A1})$$

with the standard meaning of subindexes for partial derivatives, and $||$ is the argument. The condition $U_d = \text{Im}(d\omega/dk) = 0$ leads to

$$\partial_{k_r} \Delta_r / \partial_{\omega_r} \Delta_r = \partial_{k_r} \Delta_i / \partial_{\omega_r} \Delta_i. \quad (\text{A2})$$

Since $\omega_i = 0$, the real and imaginary sheets of $\Delta = 0$ can be visualized in the $\{\omega_r, k_r, k_i\}$ space (see figure 7 for $Oh = 0.15$ and $We = 5$). In this 3D space, equation (A2) implies that the vector

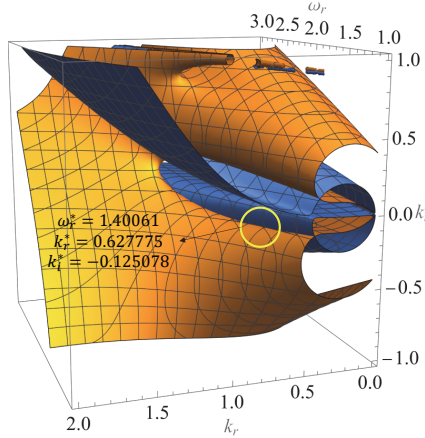


FIG. 7. Sheets of $\text{Re}(\Delta) = 0$ (blue surface) and $\text{Im}(\Delta) = 0$ (orange surface), with $\omega_i = 0$, for $Oh = 0.15$ and $We = U^2 = 5$. The intersection lines are the modes with zero local variation of their amplitude. Marked at the center of the yellow circle is the mode where $U_d = \text{Im}(d\omega/dk) = 0$ (DIM), with its corresponding values of ω_r^* , k_r^* and k_i^* . The horizontal lines ($k_i = \text{const.}$) of the orange surface indicate that $-k_i^*$ is maximum (k_i^* minimum) at that point.

product of the normal vectors to both sheets (i.e. $\{\partial_{\omega_r} \Delta_r, \partial_{k_r} \Delta_r, \partial_{k_i} \Delta_r\} \times \{\partial_{\omega_r} \Delta_i, \partial_{k_r} \Delta_i, \partial_{k_i} \Delta_i\}$) has a null component in the k_i -direction at the point of the intersection curve $k_i = k_i(\omega_r, k_r)$ where $U_d = \text{Im}(d\omega/dk) = 0$. Thus, k_i has an extreme value at that point.

¹J. Eggers and E. Villermaux, “Physics of liquid jets,” Rep. Prog. Phys. **71**, 036601 (2008).

²J. M. Montanero and A. M. Gañán-Calvo, “Dripping, jetting and tip streaming,” Rep. Prog. Phys. **83**, 097001 (2020).

³C. Weber, “Zum zerfall eines flüssigkeitsstrahles (on the breakup of a liquid jet),” ZAMP **11**, 136–159 (1931).

⁴S. Chandrasekhar, *Hydrodynamic and hydromagnetic stability* (Dover, New York, USA, 1961).

⁵J. B. Keller, “Spatial instability of a jet,” Phys. Fluids **16**, 2052–2055 (1973).

⁶L. Brillouin, *Wave propagation and group velocity* (Academic Press, New York, USA, 1960).

⁷G. Whitham, *Linear and nonlinear waves* (Wiley, New York, USA, 1974).

⁸L. Muschietti and C. T. Dum, “Real group velocity in a medium with dissipation,” Phys. Fluids. B **5**, 1383 (1993).

- ⁹V. Gerasik and M. Stastna, “Complex group velocity and energy transport in absorbing media,” *Phys. Rev. E* **81**, 056602 (2010).
- ¹⁰R. J. Briggs, *Electron-Stream Interaction with Plasmas* (MIT Press, Cambridge, 1964).
- ¹¹P. Huerre and P. A. Monkewitz, “Local and global instabilities in spatially developing flows,” *Annu. Rev. Fluid Mech.* **22**, 473–537 (1990).
- ¹²W. V. Sarloos, “Front propagation into unstable states,” *Phys. Rep.* **386**, 29–222 (2003).
- ¹³S. J. Leib and M. E. Goldstein, “Convective and absolute instability of a viscous liquid jet,” *Phys. Fluids* **29**, 952–954 (1986).
- ¹⁴S. J. Leib and M. E. Goldstein, “The generation of a capillary instability on a liquid jet,” *J. Fluid Mech.* **168**, 479–500 (1986).
- ¹⁵A. M. Gañán-Calvo, H. N. Chapman, M. Heymann, M. O. Wiedorn, J. Knoska, B. Gañán-Riesco, J. M. López-Herrera, F. Cruz-Mazo, M. A. Herrada, J. M. Montanero, and S. Bajt, “The natural breakup length of a steady capillary jet: Application to serial femtosecond crystallography,” *Crystals* **11**, 990 (2021).
- ¹⁶W. K. Bani and M. C. Mahato, “An experimental study of recoil capillary waves and break up of vertically flowing down water jets,” *Pramana - J Phys* **95** (2021).
- ¹⁷A. Umemura, “Self-destabilising loop of a low-speed water jet emanating from an orifice in microgravity,” *J. Fluid Mech.* **797**, 146–180 (2016).
- ¹⁸A. Umemura, J. Osaka, J. Shinjo, Y. Nakamura, S. Matsumoto, M. Kikuchi, T. Taguchi, H. Ohkuma, T. Dohkojima, T. Shimaoka, T. Sone, H. Nakagami, and W. Ono, “Coherent capillary wave structure revealed by iss experiments for spontaneous nozzle jet disintegration,” *Microgravity Science and Technology* **32**, 369–397 (2020).
- ¹⁹H. Liu, Z. Wang, L. Gao, Y. Huang, H. Tang, X. Zhao, , and W. Deng, “Optofluidic resonance of a transparent liquid jet excited by a continuous wave laser,” *Phys. Rev. Lett.* **121**, 244502 (2021).
- ²⁰R. P. Grant, *Newtonian jet stability*, Ph.D. thesis (1965).
- ²¹R. P. Grant and S. Middleman, “Newtonian jet stability,” *AIChE J.* **12**, 669–678 (1966).
- ²²R. W. Fenn and S. Middleman, “Newtonian jet stability: the role of air resistance,” *A.I.Ch.E. J.* **15**, 379–383 (1969).
- ²³S. A. Berger, “Initial-value stability analysis of a liquid jet,” *SIAM J. Appl. Maths* **48**, 973–991 (1988).
- ²⁴N. Ashgriz and F. Mashayek, “Temporal analysis of capillary jet breakup,” *J. Fluid Mech.* **291**, 163–190 (1995).
- ²⁵J. M. López-Herrera and A. M. Gañán-Calvo, “A note on charged capillary jet breakup of conducting liquids: experimental validation of a viscous one-dimensional model,” *J. Fluid Mech.* **501**, 303–326 (2004).
- ²⁶F. García and H. Gonzalez, “Normal-mode linear analysis and initial conditions of capillary jets,” *J. Fluid Mech.* **602**, 81–117 (2008).
- ²⁷H. González and F. García, “The measurement of growth rates in capillary jets,” *J. Fluid Mech.* **619**, 179–212 (2009).
- ²⁸F. J. García, H. González, J. R. Castrejón-Pita, and A. A. Castrejón-Pita, “The breakup length of harmonically stimulated capillary jets,” *App. Phys. Lett.* **105**, 094104 (2014).
- ²⁹L. Rayleigh, “On the instability of jets,” *Proc. London Math. Soc.* **s1-10**, 4–13 (1878).
- ³⁰T. Si, F. Li, X.-Y. Yin, and X.-Z. Yin, “Spatial instability of coflowing liquid-gas jets in capillary flow focusing,” *Phys. Fluids* **22**, 112105 (2010).